Università degli Studi di Padova

Padua Research Archive - Institutional Repository

Reactive deposition of NiO ultrathin films on Pd(100)

Original Citation:

Availability:
This version is available at: 11577/2450415 since:

Publisher:
ELSEVIER SCIENCE SA LAUSANNE, PO BOX 564, 1001 LAUSANNE 1, SWITZERLAND

Published version:
DOI: 10.1016/j.susc.2004.07.033

Terms of use:
Open Access

This article is made available under terms and conditions applicable to Open Access Guidelines, as described at http://www.unipd.it/download/file/fid/55401 (Italian only)

(Article begins on next page)

ELSEVIER

Available online at www.sciencedirect.com

SCIENCE DIRECT®

Surface Science 569 (2004) 105–117

www.elsevier.com/locate/susc

Reactive deposition of NiO ultrathin films on Pd(1 0 0)

T. Orzali, S. Agnoli, M. Sambi *, G. Granozzi

Unità di Ricerca INFM and Dipartimento di Scienze Chimiche, Università di Padova, Via Marzolo 1, I-35131 Padova, Italy

Received 8 June 2004; accepted for publication 26 July 2004
Available online 12 August 2004

Abstract

NiO ultrathin films have been grown on Pd(1 0 0) following a reactive deposition procedure. Ni has been dosed at room temperature on the substrate surface in an oxygen partial pressure of 4×10^{-6} mbar. The electronic and structural evolution of the resulting NiO(1 0 0) ultrathin films has been followed by means of X-ray photoelectron spectroscopy (XPS), X-ray photoelectron diffraction (XPD), low energy electron diffraction (LEED), and scanning tunnelling microscopy (STM). XPS, XPD and STM data indicate a 2D growth of the first NiO monolayer, while further growth leads to the nucleation of 3D islands, in a Stranski–Krastanov growth scheme. Combined XPD and LEED data indicate an initially pseudomorphic growth, characterised by in-plane compressive tetragonal strain of the NiO film, with a consequent out-of-plane interlayer expansion. Partial strain relaxation occurs abruptly, very likely between the second and the third atomic layer of the 3D islands, while a completely bulk-like cubic environment is reached only gradually as a function of thickness. NiO(1 0 0) films even ~50 equivalent monolayers thick can be grown with good long-range order, as shown by (1×1) LEED images.
© 2004 Elsevier B.V. All rights reserved.

Keywords: Nickel oxides; Palladium; Epitaxy; X-ray photoelectron spectroscopy; Low energy electron diffraction (LEED); Scanning tunneling microscopy; X-ray scattering, diffraction, and reflection

1. Introduction

Ultrathin NiO films deposited on different substrates have become an increasingly appealing field of research in recent years [1–13]. The reasons for such an interest are partly due to fundamental issues related to the electronic structure of 2D oxide overlayers grown on an oxide or a metal substrate. As a matter of fact, when dealing with metallic substrates, the interplay between the reduced dimensionality of the film, the influence of the image charge potential at the interface and the hybridization of oxide and substrate states near the Fermi level have a role in determining the electronic properties and hence the reactivity of the overlayer, which can differ dramatically from those

* Corresponding author. Tel.: +39 049 827 5189; fax: +39 049 827 5161.
E-mail address: mauro.sambi@unipd.it (M. Sambi).

0039-6028/$ - see front matter © 2004 Elsevier B.V. All rights reserved.
doi:10.1016/j.susc.2004.07.033

of the bulk oxide [14]. Moreover, when transition metal oxides are concerned, the partial population of d levels often leads to peculiar magnetic properties, which can be dramatically modified in the ultrathin film regime. It has been shown recently that a single monolayer (ML) NiO film grown on Ag(1 0 0) shows strong dichroism in $L_{2,3}$ X-ray absorption (XAS) spectra, which is phenomenologically similar to the linear magnetic dichroism detected in anti-ferromagnetic (AF) thicker films, but is rather originated by crystal field effects related to the lower symmetry C_{4v} environment of Ni^{2+} ions in the monolayer film, opposed to the O_h environment for the cations in bulk NiO [15]. In addition, tetragonal strain deriving from matching pseudomorphically the NiO film (whose bulk phase is characterised by a fcc rocksalt structure) to a lattice-mismatched substrate has been shown to have consequences on the magnetic linear dichroism of the L_2 edge [16]. In particular, it has been demonstrated that the dichroic signal can be reversed for NiO(1 0 0) ultrathin films grown on materials with reversed lattice mismatch, like Ag(1 0 0) ($a_{NiO} = 4.176$ Å $> a_{Ag} = 4.086$ Å, resulting in a +2.2% lattice mismatch), thus opening new perspectives in the understanding of exchange bias and in its applications.

Recently, we have considered Pd(1 0 0) as an alternative to Ag(1 0 0) for the growth of NiO ultrathin films [17]. The NiO/Pd(1 0 0) system is characterised by a larger reversed lattice mismatch with respect to the NiO/Ag(1 0 0) interface ($a_{Pd} = 3.891$ Å, leading to a 7.3% lattice mismatch) and Pd has a valence band (VB) composed primarily by 4d states near the Fermi level, to be compared to the 5sp nature of the Ag VB in the same energy range.

Our previous work [17] was concerned with the post-oxidation (PO) growth procedure, which consists in depositing small amounts on metallic Ni in UHV conditions on the Pd substrate, followed by an annealing treatment in oxygen in order to produce the NiO overlayers. The obtained results highlighted the surprising dependence of the ultrathin film composition and structure on the Ni dose deposited at each step of the PO procedure. In particular, it has been shown that there is a critical Ni dose which is able to initiate substantial substrate oxidation during the PO treatment, which ultimately leads to amorphous overlayers. Substrate oxidation can be avoided by preventing the formation of a direct metal–metal interface. This can be accomplished by presaturating the Pd surface with oxygen, so to get the $(\sqrt{5} \times \sqrt{5})$-R27°-O/Pd(1 0 0) structure [18,19]. When the "$\sqrt{5}$" structure is used as the starting point for the PO growth procedure, NiO(1 0 0) ultrathin films with moderate long-range order and with good compositional homogeneity as a function of thickness can be obtained, with no substrate oxidation.

In the present paper we report on the alternative growth procedure consisting in reactive deposition (RD), where Ni is dosed on the Pd substrate at room temperature (RT) in the presence of an oxygen background pressure. We show that NiO ultrathin films up to several tens of ML thick can be obtained following this route, characterised by a better developed long-range order with respect to the PO procedure. Information on the growth mode and strain relaxation is also derived by combining STM, photoelectron and low energy electron diffraction measurements.

2. Experimental

Sample treatments were performed in an UHV preparation chamber at a base pressure of 5×10^{-11} mbar. The Pd(1 0 0) crystal was cleaned by repeated cycles of argon ion sputtering (KE = 2 keV), and annealing at $T = 970$ K with a final flash in 1×10^{-6} mbar O_2 (uncorrected ion gauge reading). The exposure to oxygen ensured the removal of the carbon contaminant segregating to the surface during each annealing cycle, and left the surface free from either C or O, as judged by grazing angle XPS measurements. The cleaning cycles were repeated until a sharp (1×1) LEED (VG Microtech Rear View LEED—RVL900) pattern was observed and a good anisotropy developed in Pd 3d XPD scans (anisotropy $\chi = (I_{max} - I_{min})/I_{max}$, with I_{max} and I_{min} being respectively the maximum and minimum values of the photoelectron intensity detected in a scan).

NiO layers were grown following a RD procedure: Ni was deposited at RT by means of an

electron beam evaporator (Omicron EFM) in an oxygen partial pressure of 4×10^{-6} mbar (residual gas analyser reading). An annealing treatment at 473 K in an oxygen partial pressure of 5×10^{-7} mbar following the deposition was occasionally performed for low coverages (~1 ML) in order to improve the long-range order of the deposited layer, leading to a $c(4 \times 2)$ LEED pattern (see below). The deposition rate of NiO resulting from such treatments was estimated to be $\sim 2.2 \pm 0.1$ Å/min, as determined by angle resolved XPS [17,20] and quartz microbalance calibrations. Thickness values expressed in ML equivalents (ML_{eq}) are calculated assuming an interlayer distance between adjacent planes in NiO(1 0 0) equal to 2.09 Å. Thicknesses investigated in the present work correspond to 1, 2, 5, 8, 10, 15, 20 and 46 ML_{eq}.

XPS and XPD data were collected using a modified VG ESCALAB MKII photoelectron spectrometer. The sample was mounted on a two-axis goniometer which allowed the sweeping of the electron emission direction with an angular resolution of ±1° both in polar angle (θ, defined with respect to the surface normal) and in azimuthal angle (ϕ, defined with respect to the [0 1 1] direction on the surface). The acceptance half-angle of the electron analyser was estimated to be 3.5°.

All relevant XPS features were acquired at near normal ($\theta = 24°$) and grazing ($\theta = 72°$) emission, in order to probe the compositional homogeneity of the NiO overlayers as a function of thickness. True normal emission was avoided to prevent possible distortions due to strong along-normal forward scattering (FS) effects. The MgKα source with a pass energy (PE) of 20 eV was used throughout the XPS experiments. Sufficient resolution is thereby achieved to be able to highlight the fine structure evolution in Ni 2p spectra as a function of thickness.

XPD scans for structural analysis were obtained for Pd 3d emission from the clean substrate and for Ni $2p_{3/2}$ photoelectron and O KLL Auger emission from NiO ultrathin films as a function of overlayer thickness. Line intensities are reported after a simple linear background subtraction. Unmonochromatized AlKα radiation was used for the XPD experiments. The O KLL Auger line has been used for monitoring oxygen because the O 1s peak is partially superimposed to the Pd $3p_{1/2}$ feature of the substrate.

STM experiments were performed in a custom designed three-chamber UHV system operating at a base pressure of 1×10^{-10}. The STM (Oxford Instruments) has been operated at room temperature (RT) in a constant current mode.

3. Results

3.1. XPS data

Fig. 1 shows the Ni 2p photoemission line from NiO deposited reactively on Pd(1 0 0) as a function of the overlayer thickness at near-normal and grazing emission. Fig. 2 shows the Pd 3d peak from the clean substrate (dashed line) and from the Pd(1 0 0) crystal covered by a 5 ML_{eq} thick NiO film (full line), measured at grazing emission.

The following observations can be made:

- The full width at half maximum (FWHM) of the two main components of the Ni 2p doublet reaches a maximum with the third ML_{eq}, while it decreases to an almost constant value starting from the fifth ML_{eq}.
- The Ni $2p_{3/2}$ component undergoes a shift of 1.8 eV (from 852.2 to 854.0 eV) on going from 1 to 46 ML_{eq}. The Ni $2p_{1/2}$ component shifts by 2.4 eV (from 869.8 to 872.2 eV) in the same thickness range. Most of the shift occurs within the first 5 ML_{eq}: while the binding energy (BE) of the two components remains constant for the first 2 ML_{eq}, a clear shift is observed starting from the third ML_{eq} and the steady-state, bulk-like value is reached with the fifth ML_{eq}. The measured shifts do not depend on the acquisition angle.
- The BE separation between the Ni $2p_{3/2}$ photoemission line and its main satellite is 8.8 eV for 1 and 2 ML_{eq} thick NiO films; it becomes 7.0 eV for thicker layers. As far as the Ni $2p_{1/2}$ peak and its satellite are concerned, the BE separation goes from 10.8 to 8.6 eV.

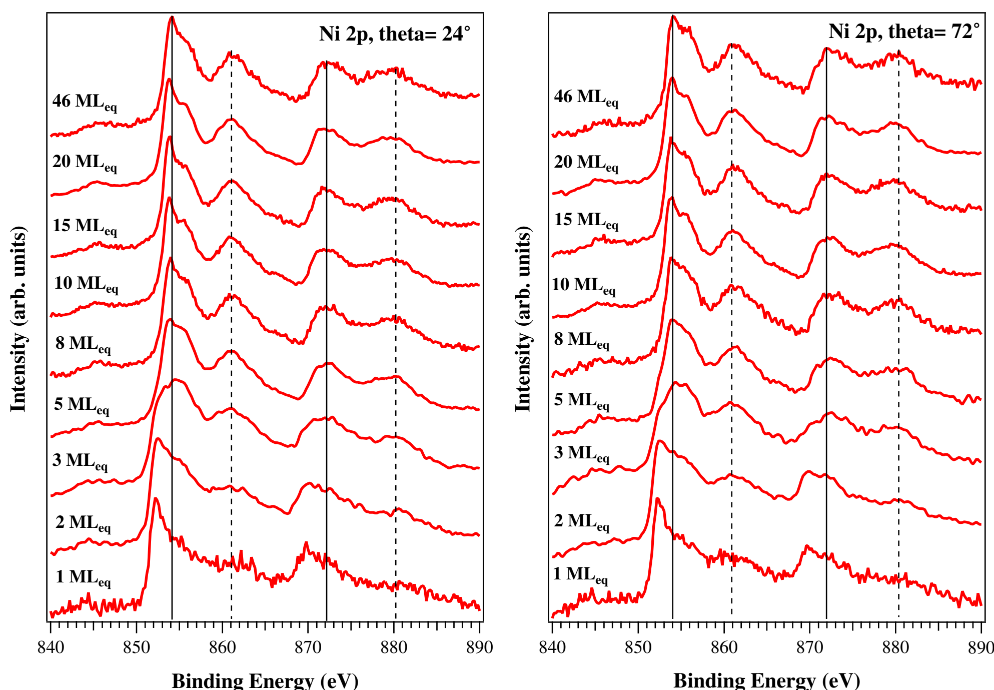

Fig. 1. Ni 2p XPS photoemission lines acquired on NiO/Pd(1 0 0) as a function of thickness, at $\theta = 24°$ (left) and at $\theta = 72°$ (right) with respect to the sample normal. Full vertical lines indicate the BE positions of the bulk doublet components; dashed vertical lines are placed at the expected BE values for the bulk main satellite lines. The MgKα source was used for acquisition.

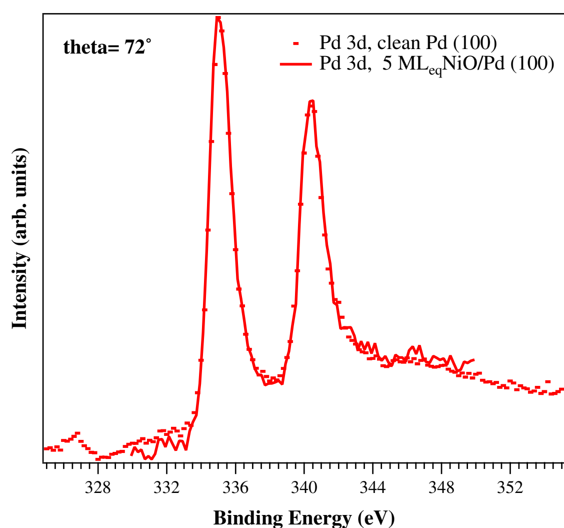

Fig. 2. Pd 3d photoemission line at $\theta = 72°$ acquired on the clean substrate (dots) and on Pd covered by 5 ML$_{eq}$ of NiO (full line). Spectra have been normalized to the same intensity in order to point out directly possible changes in the FWHM.

- The intensity ratio between the satellites and the respective main peaks grows as a function of thickness, while the FWHM of the satellites decreases. Stable values are reached with the fifth ML$_{eq}$.
- Multiplet splitting of the Ni $2p_{3/2}$ line, typical of long-range ordered bulk-like NiO [9,17] is absent in the 1 ML$_{eq}$ film. It starts to develop in the 2 ML$_{eq}$ thick film, it is not easily discernible in the 3 ML$_{eq}$ film due to the transition (to be detailed later) occurring at this thickness, and it finally reaches the appearance of bulk-like NiO starting from the fifth ML$_{eq}$.
- No substantial oxidation of the substrate is apparent from data reported in Fig. 2 as the deposition proceeds: the FWHM of both Pd 3d doublet components do not change with NiO exposure. This points out an important difference from what happens with the PO growth procedure, where substantial Pd oxidation

occurs if no oxygen presaturation of the substrate surface is performed prior to the NiO growth [17].

3.2. XPD data

Figs. 3 and 4 show polar Ni 2p photoelectron diffraction (PPD) scans along the [0 0 1] and [0 1 1] main substrate azimuths, acquired as a function of thickness with the AlKα source. Fig. 3 displays the low coverage curves, up to 5 ML_{eq}, normalized with respect to the 1/cosθ response typical of ultrathin films [20]. Curves referring to thicker layers are reported in Fig. 4.

Ni 2p and O KLL azimuthal photoelectron diffraction (APD) scans at the polar angle $\theta = 45°$ as a function of thickness are reported in Fig. 5, along with their anisotropy as a function of thickness. Both PPD and APD scans show a gradual development of the diffraction features peculiar to a (1 0 0) oriented rocksalt structure [17]. In particular, curves referring to the 1 ML_{eq} coverage are almost structureless, thus confirming the 2D growth mode of the first deposited monolayer. The 2 ML_{eq} polar scans, besides weak off-normal features, show clearly the onset of along-normal FS.

Important information is conveyed by the 3 and 5 ML_{eq} Ni 2p polar scans along both azimuths (Fig. 3): although FS peaks are very broad, which is indicative of a complex mixture of locally slightly different environments, a clear shift of the main off-normal FS features toward more grazing angles is observed in this thickness range. In particular, the peaks which are found at $\theta = 16°$ and 40° in the 3

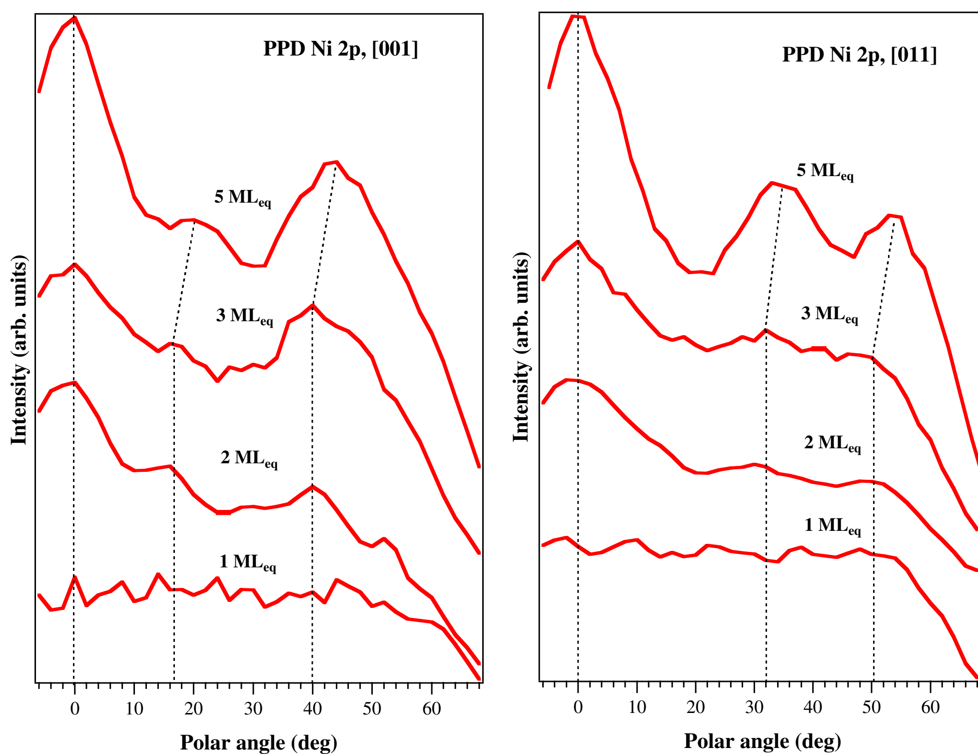

Fig. 3. Polar photoelectron diffraction (PPD) scans on Ni 2p along two main substrate azimuthal directions for the thickness interval 1–5 ML_{eq}. Dashed lines indicate the occurrence of main forward scattering directions. Out-of-plane interlayer contraction between 3 and 5 ML_{eq} is highlighted by bending the off-normal dashed lines. The kinetic energy of outgoing photoelectrons is KE ~ 635 eV. Scans have been normalized with respect to the 1/cosθ response typical of ultrathin films.

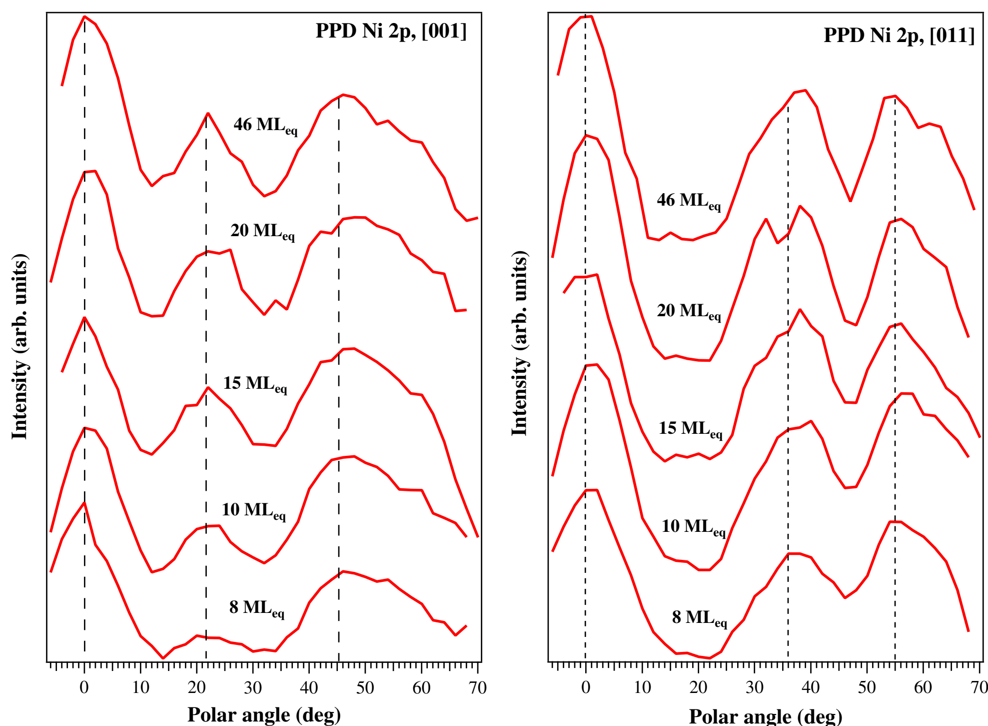

Fig. 4. Polar photoelectron diffraction (PPD) scans on Ni 2p along two main substrate azimuthal directions for the thickness interval 8–46 ML$_{eq}$. Dashed lines indicate the occurrence of main forward scattering directions in bulk NiO(100). KE ~ 635 eV.

ML$_{eq}$ curve along the [001] azimuth shift to $\theta = 20°$ and 45° respectively in the 5 ML$_{eq}$ curve. Similarly, along the [011] substrate azimuth the peaks centered at $\theta = 32°$ and 50° shift to $\theta = 35°$ and 55°, respectively, which are the bulk-like values for NiO(100). This shift is paralleled by a more than 10% increase of azimuthal curves anisotropies between 3 and 5 ML$_{eq}$ (see Fig. 5, right panel). Further growth simply increases the anisotropy of polar scans and enriches to some extent their fine structure, with no further major changes in position or relative intensities.

Finally, Fig. 6 shows the Ni 2p$_{3/2}$ and O KLL 2π plots acquired on a 20 ML$_{eq}$ thick NiO film. Both plots are characterised by fourfold symmetry and by very similar diffraction features.

3.3. LEED data

LEED images acquired on NiO ultrathin films grown on Pd(100) as a function of thickness are reported in Figs. 7 and 8. The energy of the electron beam is generally set at 70 eV, with a few small exceptions. For the 2, 3 and 5 ML$_{eq}$ thick films, data acquired at $E = 88$ eV are also reported.

The 1 ML$_{eq}$ pattern (Fig. 7a) shows a rather sharp (1 × 1) periodicity. A very faint c(4 × 2) superstructure was observable in the very initial stages of the LEED image acquisition, which quickly faded away, presumably under the effect of the electron beam. Interestingly enough, a post-annealing in oxygen (partial pressure of $p = 5 \times 10^{-7}$ mbar) at $T = 473$ K leads to a very sharp and stable c(4 × 2) superstructure (Fig. 7b), which is of the same pattern obtained by dosing Ni on the ($\sqrt{5} \times \sqrt{5}$)-R27°-O/Pd(100) structure in the PO growth procedure with oxygen presaturation [17]. A thorough investigation of the c(4 × 2) phase, including STM data, will be discussed in a forthcoming paper [21].

If RD is continued up to 2 ML$_{eq}$ (without prior post-annealing of the 1 ML$_{eq}$ layer: Fig. 7c and d;

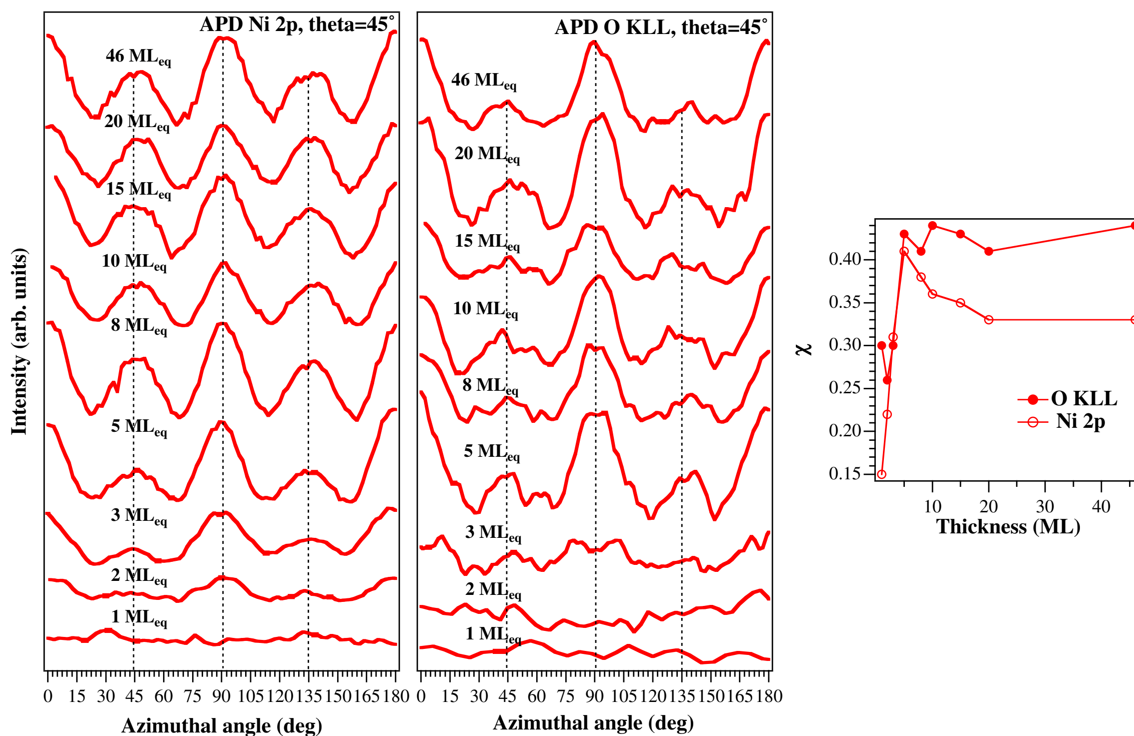

Fig. 5. Azimuthal photoelectron diffraction (APD) scans on Ni 2p (left, KE ~ 635 eV) and O KLL (center, KE ~ 510 eV), taken at $\theta = 45°$ as a function of the NiO ultrathin film thickness. Anisotropy χ of Ni 2p and O KLL azimuthal scans at $\theta = 45°$ as a function of the overlayer thickness (right).

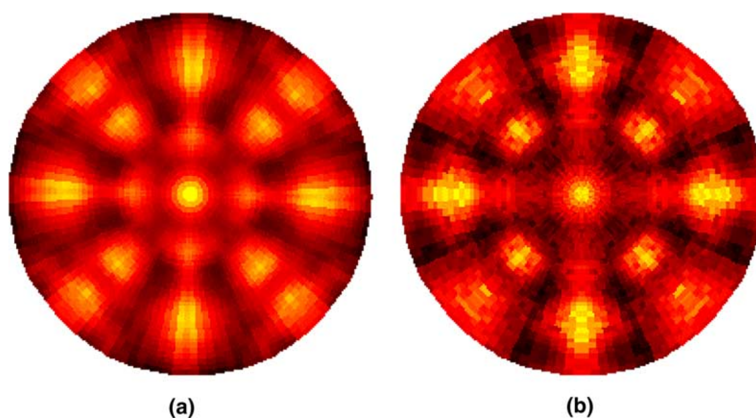

Fig. 6. (a) Ni $2p_{3/2}$ (KE ~ 632 eV) and (b) O KLL (KE ~ 510 eV) 2π plots from the 20 ML$_{eq}$ thick NiO film on Pd(100). The maximum off-normal θ value is 70°. The [001] substrate main azimuth corresponds to the horizontal radius pointing to the right.

after post-annealing, i.e. starting from the c(4 × 2) phase: Fig. 7e) a (1 × 1) structure is observed, which however shows a spot splitting towards the specular beam (hidden by the electron gun in our rear-view geometry). The splitting, which indicates a shrinkage of the first Brillouin zone (BZ)

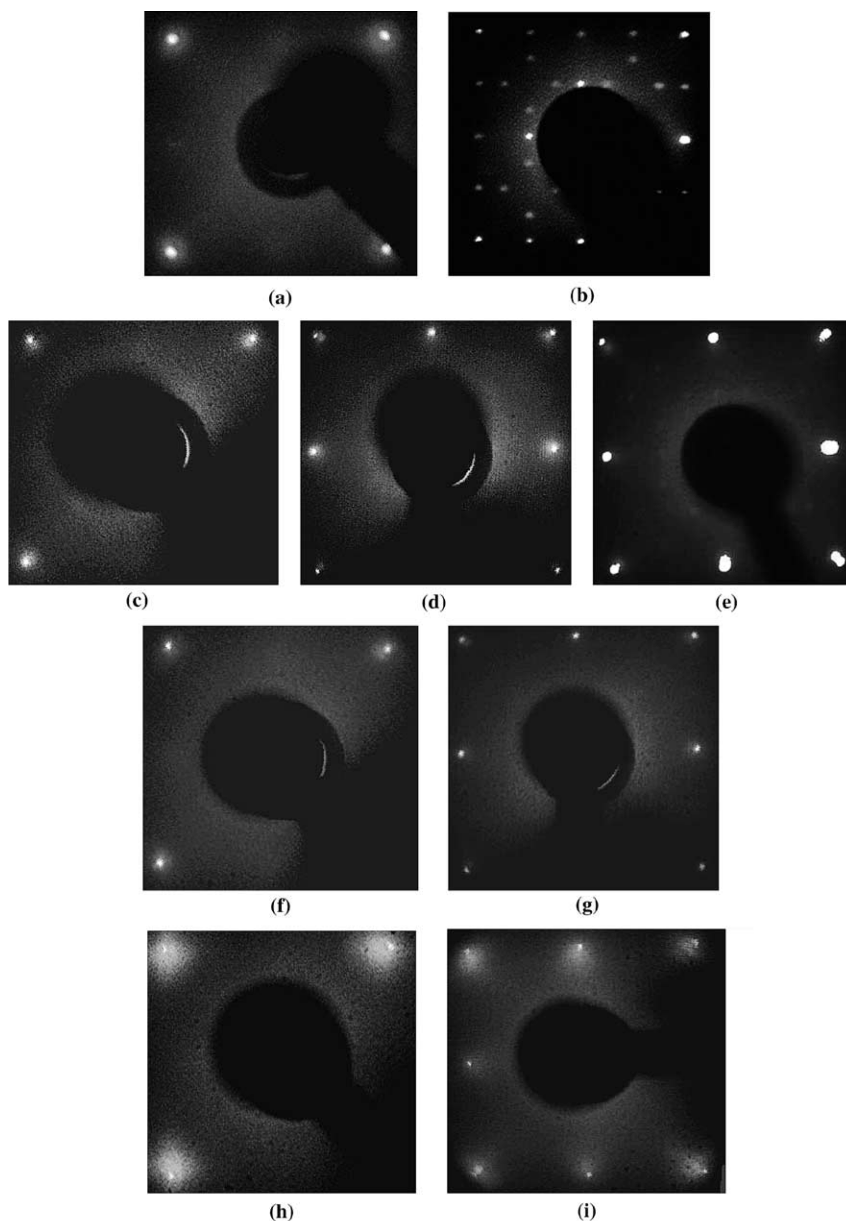

Fig. 7. LEED patterns of NiO ultrathin films as a function of thickness in the 1–5 ML_{eq} range: (a) 1 ML_{eq}, $E = 70$ eV; (b) 1 ML_{eq}, c(4 × 2) phase obtained by post-annealing at 473 K in 5×10^{-7} mbar O_2, $E = 134$ eV; (c) 2 ML_{eq}, $E = 70$ eV; (d) 2 ML_{eq}, $E = 88$ eV; (e) 1 ML_{eq}, c(4 × 2) phase + 1 ML_{eq}, $E = 93$ eV; (f) 3 ML_{eq}, $E = 70$ eV; (g) 3 ML_{eq}, $E = 88$ eV; (h) 5 ML_{eq}, $E = 66$ eV; (i) 5 ML_{eq}, $E = 88$ eV.

for a number of atomic layers above a certain value, is observed up to a thickness of 5 ML_{eq}, although the splitting becomes less resolved as thickness increases (Fig. 7h and i). A quantitative measurement of the splitting is made difficult by the rather low resolution of the standard LEED equipment. However, a 3.5% shortening of the reciprocal unit cell side can be estimated rather

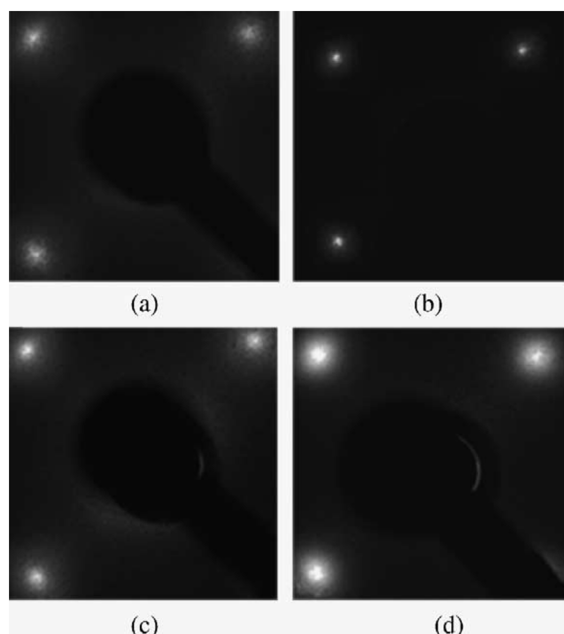

Fig. 8. LEED patterns of NiO ultrathin films as a function of thickness in the 10–46 ML_{eq} range: (a) 10 ML_{eq}, $E = 70$ eV; (b) 15 ML_{eq}, $E = 70$ eV; (c) 20 ML_{eq}, $E = 74$ eV; (d) 46 ML_{eq}, $E = 67$ eV.

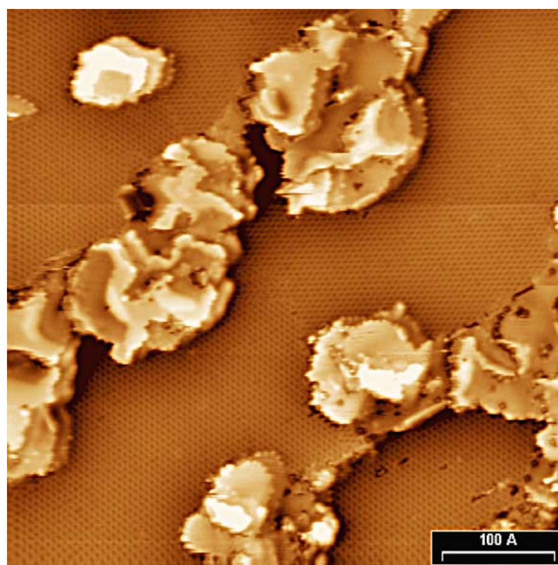

Fig. 9. STM image of 1.7 ML_{eq} NiO deposited on Pd(1 0 0). 500 Å × 500 Å, $I = 0.2$ nA, $V = -2.0$ V.

accurately from the 2 ML_{eq} LEED image by measuring the distance between the $(-1,-1)$ and the $(1,1)$ and between the $(-1,1)$ and $(1,-1)$ split spots. This contraction in the first BZ corresponds to a 3.6% in-plane expansion of the real lattice.

The thicker layers observed with LEED (Fig. 8a–d) show a simple (1×1) structure with broadened spots, which however is clearly seen even for the thickest layer considered in our investigation (46 ML_{eq}).

3.4. STM data

Fig. 9 shows an STM image of 1.7 ML_{eq} NiO grown on Pd(1 0 0). The deposition was performed at RT at a rate of 0.8 ML_{eq}/min in an oxygen background ($p(O_2) = 2\times10^{-6}$ mbar) and followed by two annealing cycles (at $T = 473$ and 573 K, respectively) in oxygen ($p(O_2) = 5\times10^{-7}$ mbar).

The wetting and long-range ordered $c(4\times2)$ phase developed by the first Ni ML is clearly seen in the image. The NiO dose exceeding the single ML grows as 3D islands up to three atomic layers thick.

4. Discussion

It has been shown recently that the Ni 2p XPS threshold from a 2D NiO single ML on the Ag(1 0 0) metallic substrate differs substantially from the analogous feature from bulk NiO, being more similar to—though with significant differences—the metal case [9]. Reasons for such a behaviour can be traced back to the reduction of Coulomb and charge transfer energies in the metal-supported thin film with respect to the bulk oxide due to the image charge potential, coupled with the hybridization of the oxide electronic structure with the substrate states close to the Fermi level [14,22]. The Ni 2p feature measured from our NiO 1 ML_{eq} on Pd(1 0 0) resembles the analogous data collected from the NiO ML deposited on Ag(1 0 0) [9]. In particular, the BE energy of the two main components are intermediate between the reference values for metallic Ni and NiO, the separation between the main lines and the respective satellites is larger than in metallic

nickel, while the satellite intensities are considerably weaker than in bulk nickel oxide. Moreover, the main lines do not show the multiplet splitting which, in bulk-like NiO is due to 2p–3d hole–hole interactions and possibly to Ni–Ni intersite interactions known as non-local screening [23]. In summary, the 1 ML_{eq} thick NiO film deposited on Pd(1 0 0), judging from the Ni 2p XPS feature, appears to grow as a wetting 2D overlayer. Further evidence for this suggestion will be given by XPD data.

The incipient appearance of the multiplet splitting in the Ni $2p_{3/2}$ line and the intensity increase of the satellites already for the 2 ML_{eq} thick overlayer seems to point out a change in the growth mode from 2D wetting to 3D clustering, a suggestion which is strengthened by XPD data, as will be seen below. The peculiar shape of the 3 ML_{eq} spectrum, on the other hand, can be correlated to the strain relaxation of the initially pseudomorphic, tetragonally distorted NiO overlayer to a relaxed, more bulk-like oxide lattice, which is demonstrated by both LEED and XPD measurements. The typical features of long-range ordered, bulk-like NiO are henceforth maintained up to substantial thickness values, and are always accompanied by a clear (1×1) LEED pattern, albeit the more diffuse the larger the thickness (Fig. 7).

An important observation is the absence of substrate oxidation during the RD procedure, as opposed to the PO procedure without substrate oxygen presaturation (Fig. 2). In our previous work on the PO growth [17] we have shown that Pd oxidation critically depends upon the quantity of metallic nickel that is put in contact with the clean Pd surface during the first Ni dose. When such critical value is used, subsequent PO leads to substantial substrate oxidation and eventually to the amorphization of the interface. These observations gave convincing evidence that metallic Ni at a particular coverage acts as a promoter of Pd oxidation, which can therefore be avoided by preventing the formation of a direct Ni/Pd interface, notably by presaturating the Pd surface with the $(\sqrt{5} \times \sqrt{5})$-R27° oxygen superstructure. In the present RD experiment no Pd oxidation is observed even in the absence of oxygen presaturation, which suggests that Ni oxidation occurs readily on the substrate as soon as the reactants meet on the surface, i.e. no stable Ni metallic clusters having the critical size necessary to initiate substrate oxidation.

XPD data reported in Figs. 3–5 give further support to the Stranski–Krastanov growth mode suggested by XPS results. Curves referring to the single ML_{eq} are almost structureless. The 1 ML_{eq} azimuthal scans reported in Fig. 5 are particularly clear in this respect: no structure at all is seen in both Ni 2p and O KLL azimuthal scans at $\theta = 45°$, which indicates the absence of scatterers in the plane above the photoelectron emitters at a polar angle where strong FS events are expected for a (1 0 0)-oriented NaCl lattice structure. The 1 ML_{eq} polar scans normalized with respect to the $1/\cos\theta$ response typical of ultrathin thin films give similar information: no FS peaks are detected in the whole polar angle range, thus confirming the 2D growth habit of the overlayer in the single monolayer regime.

Ni 2p polar curves along the substrate main azimuths referring to 2 ML_{eq} (Fig. 3), besides showing the FS events which would be expected for an actual thickness of 2 ML NiO(1 0 0) (at $\theta = 45°$ along [0 0 1], at $\theta = 55°$ along [0 1 1] and at $\theta = 0°$ along the normal to the surface for an undistorted, bulk-like arrangement; at $\theta = 40°$ along [0 0 1] and at $\theta = 50°$ in the presence of substantial compressive tetragonal strain, as in the present case), also display an additional faint peak along the [0 0 1] polar scan at $\theta \sim 16$–18°, which shifts to higher polar angles and becomes more intense for thicker layers (see Fig. 4, left panel). In a NaCl-like structure along the [0 0 1] azimuth, a Ni–Ni FS event is expected at $\theta = 18.4°$ and a weaker Ni–O FS peak occurs at $\theta = 26.6°$. These FS features can be expected only for layers at least 4 and 3 ML thick, respectively (as a matter of fact, in polar scans from thicker layers—Fig. 4—a single peak is detected at $\theta \sim 22°$, which is a convolution of the two mentioned features, given our experimental angular resolution, which is estimated to be approximately ±3.5°). In addition, in the 2 ML_{eq} polar scan along the [0 1 1] azimuth (Fig. 3, right panel), a faint peak is detected at $\theta \sim 30$–32°, which corresponds to the Ni–Ni FS peak at $\theta = 35.3°$ in the bulk-like rocksalt environ-

ment for layers at least 3 ML thick. In summary, the 2 ML_{eq} polar data support a strong clustering of the second deposited equivalent monolayer, so to give 3D features on the initially wetting monolayer. A definitive confirmation of the SK growth mode is given by the STM image reported in Fig. 9, where up to three atomic layers can be counted on the 3D islands nucleating on the wetting $c(4\times2)$ phase for a nominal coverage of only 1.7 ML_{eq}.

Ni 2p polar scans along both main substrate azimuthal directions for 2, 3 and 5 ML_{eq} films (Fig. 3) and Ni 2p and O KLL azimuthal scans at $\theta = 45°$ (Fig. 5) should be read in parallel with the LEED patterns referring to the same coverages, reported in Fig. 7. The XPS Ni 2p peak lineshapes of Fig. 1, already discussed above, should also be considered. A clear shift of the main FS features in PPD scans along both main azimuths at more grazing angles is observed on going from 3 to 5 ML_{eq}, as already specified in Section 3.2. At the same time, a spot splitting indicating the shrinkage of the first BZ is observed in LEED images, starting from the 2 ML_{eq} patterns (Fig. 7c–d). In other words, there is converging evidence for the occurrence of strain relaxation, with the system evolving from a pseudomorphic NiO overlayer affected by in-plane compressive strain and out-of-plane interlayer expansion, towards a more bulk-like NiO structural environment, characterised by a partial strain relaxation. The sudden increase in the anisotropy of azimuthal scans measured at $\theta = 45°$ starting from the 5 ML_{eq} thick film (Fig. 5) is also explained by strain relaxation. A significant fraction of Ni–Ni and O–O nearest neighbour directions along the [001] and symmetry-equivalent azimuths—initially found at angles higher than $\theta = 45°$ due to the interlayer expansion—become closer to $\theta = 45°$ after the strain relaxation and thus contribute more effectively to the modulation of the APD curves. A partial strain relaxation is suggested by the quantitative LEED estimate of a 3.6% in-plane lattice parameter expansion at the transition, while the lattice mismatch between bulk Pd(100) and bulk NiO(100) amounts to 7.3%.

The fact that the in-plane collapse is obvious from LEED already starting from the 2 ML_{eq} overlayer, while it becomes apparent in XPD after the third ML_{eq}, can be attributed to the different sampling depth of the two techniques coupled with the SK growth mode of the overlayer. While in LEED almost only the two topmost layers contributes to the detected intensity, all layers contribute to the XPD signal at the given kinetic energy of outgoing Ni 2p photoelectrons (KE $\sim$ 635 eV). PPD scans are therefore an average produced by the interfacial strained layers *and* by the topmost relaxed layers. In order to appreciate the contribution of the unstrained layers in a FS geometry, their weight should be comparable to the weight of the strained portion, and this happens when the relaxed part is at least *two* atomic layers thick and its population is a substantial fraction of the strained part. This explains the delay with which one observes the transition with XPD with respect to LEED. In fact, the latter is able to sample the transition when it involves a sufficient population of *single* unstrained atomic layers. Moreover, the fact that the spot splitting in LEED is observed in a whole thickness range (at least from 2 to 5 ML_{eq}) can be reconciled with the SK growth mode if one supposes that the transition starts at a precise thickness of the 3D islands. XPD and LEED taken together seem to suggest that this thickness is between 2 and 3 atomic layers: at 2 ML_{eq}, given the SK growth mode, there is *already* a sufficient population of 3 atomic layers thick islands (with the third layer relaxed) capable of producing the spot splitting; at 5 ML_{eq} (and most likely also above this value), there is *still* an appreciable fraction of 3 atomic layers thick island portions producing the residual spot splitting, which is however less resolved as the thickness increases—an indication of increasing structural disorder arising from the rather continuous relaxation of the residual strain in islands thicker than 3 atomic layers. The smooth relaxation towards the bulk-like aspect ratio of the NiO structure could also be responsible for the rather broad FS peaks in PPD scans below approximately 10 ML_{eq}.

The stable structure for thicker layers is certainly the bulk-like NiO(100) lattice, with a [001]||[001] epitaxial relationship with the substrate, as summarised by Ni 2p and O KLL 2π

plots reported in Fig. 6. As already discussed in Ref. [17], the very similar XPD modulations of the two signals in a FS regime marks the identity of the structural environments sampled by photoemission from both anion and cation lattice sites and are thus a reliable fingerprint of the NaCl-like lattice structure of NiO. Good LEED patterns obtained for layers several tens of ML thick give convincing evidence for better quality NiO ultrathin films obtained with the RD procedure with respect to the PO route [17].

Finally, the results reported in the present paper should be compared with the NiO/Ag(100) case, where, due to the much lower lattice mismatch, the critical thickness is ∼20 ML [3], and the growth mode is of the layer-by-layer type [7]. Another important difference with respect to the NiO/Ag(100) system concerns the thermodynamic stability and the structure of the first deposited monolayer. While on Ag(100) the epitaxial relationship is of the (1×2) type [7,8] for reactive growth in oxygen and of the (1×1) type if a stronger oxidant like NO_2 is used as the reactant [9], the (1×1) relationship for the NiO(1 ML)/Pd(100) is established for depositions at RT, but it is easily changed to a $c(4 \times 2)$ superstructure by means of a post-annealing treatment in oxygen (see Figs. 7b and 9), which is then stably maintained also by cooling down the sample again at RT. This observation seems to indicate that the (1×1) structure is formed at RT on kinetic grounds, but is thermodynamically metastable. It is worth noting that subsequent growth of NiO(100) on the $c(4 \times 2)$ phase leads to XPS, XPD and LEED results (not shown, with the exception of the LEED image shown in Fig. 7e) which are virtually indistinguishable from those reported in this paper—i.e. the presence of subsequent atomic layers leads the interfacial matching to the simple (1×1) relationship. A similar observation was made for the PO growth with oxygen presaturation, where dosing Ni on the $\sqrt{5}$ oxygen superstructure on Pd(100) leads to the growth of NiO(100) through the formation of the $c(4 \times 2)$ phase. The nature and structure of this latter phase remains an open issue, which will be dealt with in a forthcoming paper [21], based mainly on the interpretation of atomically resolved STM images.

5. Conclusion

Reactive deposition in an oxygen atmosphere of NiO ultrathin films on Pd(100) leads to epitaxial NiO(100)/Pd(100), [001]||[001], characterised by good long-range order up to thicknesses of several tens of monolayers. The first deposited monolayer grows as a 2D wetting film. Further deposition results in a SK growth mode, leading to the formation of 3D islands. Due to the rather high lattice mismatch between NiO(100) and Pd(100), pseudomorphic growth is maintained only up to the second atomic layer. Partial strain relaxation occurs between the second and the third atomic layers, while residual strain is recovered within several subsequent monolayers.

Acknowledgments

This work has been partially funded by the Italian Ministry of Instruction, University and Research (MIUR) through the fund “Programmi di ricerca di rilevante interesse nazionale” (PRIN), project title: “Nature, properties and control of oxide surface defects. An integrated approach towards defect engineering”. Prof. Falko P. Netzer (Insitute for Experimental Physics, Karl-Franzens University, Graz, Austria) is gratefully acknowledged for allowing S.A. to perform in his laboratory the STM measurement reported in Fig. 9.

References

[1] J. Wollschläger, D. Erdös, H. Goldbach, R. Höpken, K.M. Schröder, Thin Solid Films 400 (2001) 1.
[2] P. Luches, et al., Thin Solid Films 400 (2001) 139.
[3] C. Giovanardi, A. di Bona, S. Altieri, P. Luches, M. Liberati, F. Rossi, S. Valeri, Thin Solid Films 428 (2003) 195.
[4] E. Groppo, C. Prestipino, C. Lamberti, P. Luches, C. Giovanardi, F. Boscherini, J. Phys. Chem. B 107 (2003) 4597.
[5] M. Caffio, B. Cortigiani, G. Rovida, A. Atrei, C. Giovanardi, A. di Bona, S. Valeri, Surf. Sci. 531 (2003) 368.
[6] C. Lamberti, E. Groppo, C. Prestipino, S. Casassa, A.M. Ferrari, C. Pisani, C. Giovanardi, P. Luches, S. Valeri, F. Boscherini, Phys. Rev. Lett. 91 (2003) 046101.
[7] C. Giovanardi, A. di Bona, S. Valeri, Phys. Rev. B 69 (2004) 075418.

[8] M. Caffio, B. Cortigiani, G. Rovida, A. Atrei, C. Giovanardi, J. Phys. Chem. B 108 (2004) 9919.
[9] S. Altieri, PhD Thesis, Groningen, 1999.
[10] G. Chern, C. Cheng, J. Vacuum Sci. Technol. 17 (1999) 1097.
[11] S. Dubourg, J.F. Bobo, B. Warot, E. Snoeck, J.C. Ousset, Phys. Rev. B 64 (2001) 054416.
[12] C. Argile, Surf. Sci. 517 (2002) 1.
[13] O. Sakata, M.S. Yi, A. Matsuda, J. Liu, S. Sato, S. Akiba, A. Sasaki, M. Yoshimoto, Appl. Surf. Sci. 221 (2004) 450.
[14] S. Altieri, L.H. Tjeng, G.A. Sawatzky, Thin Solid Films 400 (2001) 9.
[15] M.W. Haverkort, S.I. Csiszar, Z. Hu, S. Altieri, A. Tanaka, H.H. Hsieh, H.-J. Lin, C.T. Chen, T. Hibma, L.H. Tjeng, Phys. Rev. B 69 (2004) 020408.
[16] S. Altieri, M. Finazzi, H.H. Hsieh, H.-J. Lin, C.T. Chen, T. Hibma, S. Valeri, G. Sawatzky, Phys. Rev. Lett. 91 (2003) 137201.
[17] M. Sambi, R. Sensolo, G.A. Rizzi, M. Petukhov, G. Granozzi, Surf. Sci. 537 (2003) 36.
[18] M. Saidy, O.L. Warren, P.A. Thiel, K.A.R. Mitchell, Surf. Sci. 494 (2001) L799.
[19] M. Todorova, et al., Surf. Sci. 541 (2003) 101.
[20] C.S. Fadley, Prog. Surf. Sci. 16 (1984) 275.
[21] S. Agnoli, M. Sambi, G. Granozzi, J. Schoiswohl, S. Surnev, F.P. Netzer, manuscript in preparation.
[22] S. Altieri, L.H. Tjeng, F.C. Voogt, T. Hibma, G.A. Sawatzky, Phys. Rev. B 59 (1999) R2517.
[23] M.A. van Veenendaal, G.A. Sawatzky, Phys. Rev. Lett. 70 (1993) 2459.